Received: 6 April 2017 | Accepted: 13 October 2017
DOI: 10.1002/hyp.11386

WILEY

SI URBAN HYDROLOGY

Modelling hydrological response to a fully-monitored urban bioretention cell

Ryan D. Stewart[1] | Joong Gwang Lee[2] | William D. Shuster[3] | Robert A. Darner[4]

[1] Crop and Soil Environmental Science Department, Virginia Polytechnic Institute and State University, Blacksburg, VA, USA
[2] Center for Urban Green Infrastructure Engineering, Inc., Cincinnati, OH, USA
[3] United States Environmental Protection Agency, Office of Research and Development, National Risk Management Research Laboratory, Cincinnati, OH, USA
[4] United States Geological Survey, Michigan-Ohio Water Science Center, Columbus, OH, USA

Correspondence
Ryan D. Stewart, Crop and Soil Environmental Science Department, Virginia Polytechnic Institute and State University, Blacksburg, VA, USA.
Email: rds@vt.edu

Abstract
Municipalities and agencies use green infrastructure to combat pollution and hydrological impacts (e.g., flooding) related to excess stormwater. Bioretention cells are one type of infiltration green infrastructure intervention that infiltrate and redistribute otherwise uncontrolled stormwater volume. However, the effects of these installations on the rest of the local water cycle is understudied; in particular, impacts on stormwater return flows and groundwater levels are not fully understood. In this study, full water cycle monitoring data were used to construct and calibrate a two-dimensional Richards equation model (HYDRUS-2D/3D) detailing hydrological implications of an unlined bioretention cell (Cleveland, Ohio) that accepts direct runoff from surrounding impervious surfaces. Using both preinstallation and postinstallation data, the model was used to (a) establish a mass balance to determine reduction in stormwater return flow, (b) evaluate green infrastructure effects on subsurface water dynamics, and (c) determine model sensitivity to measured soil properties. Comparisons of modelled versus observed data indicated that the model captured many hydrological aspects of the bioretention cell, including subsurface storage and transient groundwater mounding. Model outputs suggested that the bioretention cell reduced stormwater return flows into the local sewer collection system, though the extent of this benefit was attenuated during high inflow events that may have exhausted detention capacity. The model also demonstrated how, prior to bioretention cell installation, surface and subsurface hydrology were largely decoupled, whereas after installation, exfiltration from the bioretention cell activated a new groundwater dynamic. Still, the extent of groundwater mounding from the cell was limited in spatial extent and did not threaten other subsurface infrastructure. Finally, the sensitivity analysis demonstrated that the overall hydrological response was regulated by the hydraulics of the bioretention cell fill material, which controlled water entry into the system, and by the water retention parameters of the native soil, which controlled connectivity between the surface and groundwater.

KEYWORDS
bioretention cell, green infrastructure, infiltration, low impact development, stormwater, urban hydrology, water balance

1 | INTRODUCTION AND BACKGROUND

Municipalities and agencies are utilizing green infrastructure such as stormwater infiltration systems to improve water quality, reduce peak surface water flows, and avoid costs from treating stormwater (Dietz, 2007). Stormwater infiltration systems (e.g., rain gardens, bioretention basins, infiltration trenches, and wells) typically collect stormwater and then allow it to infiltrate through soils and/or other porous media (Shuster, Gehring, & Gerken, 2007). These scalable practices may provide a low cost/low maintenance means to manage stormwater volume and retain certain pollutants such as orthophosphate (Yang, Florence, McCoy, Dick, & Grewal, 2009). The performance and hydrology of stormwater infiltration units have been measured and modelled using a variety of techniques, including field-based tracers (e.g., bromide; Yang et al., 2009), water balance determined from fully-instrumented sites (Davis, 2008; Dietz & Clausen, 2005; Eger, Chandler, & Driscoll, 2017; Li, Sharkey, Hunt, & Davis, 2009; Lucke & Nichols, 2015; Toran & Jedrzejczyk, 2017; Winston, Dorsey, & Hunt, 2016), and numerical models. For the latter, the Environmental Protection Agency Storm Water Management Model (SWMM) includes specialized modules to model the hydrologic impact of low impact development infrastructure such as rain gardens (Abi Aad, Suidan, & Shuster, 2009), whereas stand-alone programs such as RECARGA (Dussaillant, Wu, & Potter, 2004) allow for exploration of design variables (e.g., layer thicknesses and hydraulic conductivities) and their effects on infiltration, storage characteristics, and overall efficiency. Other mechanistic models of stormwater infiltration units have been created using one- (Browne, Deletic, Mudd, & Fletcher, 2008; Liu & Fassman-Beck, 2017; Meng, Wang, Chen, & Zhang, 2014), two- (He & Davis, 2010; Mangangka, Liu, Egodawatta, & Goonetilleke, 2015; Newcomer, Gurdak, Sklar, & Nanus, 2014), and three-dimensional frameworks (Endreny & Collins, 2009). Model simulations attempt to represent key hydrologic processes for green infrastructure (GI) structures and can used to both improve design attributes and understand the extent to which GI practice(s) will meet water management objectives.

In fully-built urban areas, retrofitting of stormwater infrastructure is becoming more common. In particular, bioretention cells or rain gardens that receive water from roadway surfaces are being explored as ways to reduce peak flows (Liu, Chen, & Peng, 2015), lessen flood risk (Ahiablame & Shakya, 2016), and reduce total stormwater volumes within combined sewer systems. However, the functionality of such systems may be affected by their design. For example, smooth, well-maintained inlet systems may lead to more flow through the stormwater infiltration structure and thus potentially better hydraulic retention (Jarden, Jefferson, & Grieser, 2016). Likewise, the presence (or absence) and configuration of underdrain systems may also affect the retention characteristics of retro-fitted stormwater infiltration infrastructure. Jarden et al. (2016) found that including underdrain systems on stormwater infiltration structures may limit their efficacy in reducing stormwater volumes, particularly compared to units that lacked underdrainage. These findings were also shown by a subsequent modelling effort (Avellaneda, Jefferson, Grieser, & Bush, 2017). Conversely, Zhang and Chui (2017) found that the hydrological performance of bioretention basins showed little sensitivity to the presence and size of underdrain systems.

Other studies focusing on the fate of exfiltrated stormwater have shown that this water can have variable effects on stream base flow and on groundwater levels. Broadly, base flow generation is sensitive to alterations in evapotranspiration and water table levels, which may not be fully restored by installation of GI (Bhaskar, Beesley, et al., 2016; Bhaskar, Hogan, & Archfield, 2016; Bhaskar, Welty, Maxwell, & Miller, 2015). As a possible consequence of variability arising in placement and effectiveness, urban areas with GI stormwater infiltration retrofits have been observed to have both higher (Bhaskar, Beesley, et al., 2016, Bhaskar, Hogan, et al., 2016) and lower (Fanelli, Prestegaard, & Palmer, 2017) base flow volumes compared to nearby forested catchments. At both small and large scales, soil water exfiltrating from a bioretention cell and encountering a lower-permeability soil matrix may cause groundwater mounding to occur. In some urban areas, this effect may cause for concern due to potential impacts to subsurface infrastructure such as return flow to leaky wastewater conveyance with high inflow-infiltration potential, as well as potential leakage into below-grade basements. One study using scenario-testing in MODFLOW found that single stormwater infiltration cells could result in long-term groundwater mounding of >1 m compared to a baseline scenario (Endreny & Collins, 2009). Another modelling study showed that depth to water table was an important control on the size and dissipation rate of groundwater mounds (Zhang & Chui, 2017). A statistical model of the Boston, Massachusetts, area found that installation of stormwater infiltration structures resulted in a small but significant increase in groundwater levels (Thomas & Vogel, 2011). Using an array of shallow groundwater wells, Machusick, Welker, and Traver (2011) determined that groundwater mounding occurred beneath a small bioretention basin during large precipitation events, though the effects in this case were generally localized. Still, there exists considerable uncertainty regarding the extent to which small-scale stormwater infiltration systems affect water table levels, modulate flooding, or reduce return flow risk.

Altogether, the effectiveness of retrofitted stormwater infiltration systems in reducing stormwater volumes and the effects of such systems on local groundwater levels are still not well understood. The primary objective of this study was therefore to combine field data with an unsaturated-zone model to evaluate the performance of an unlined bioretention cell in reducing stormwater volume into a combined sewer system. Specifically, the study sought to address two questions: (a) To what extent can street-side stormwater infiltration systems reduce or otherwise modify inflow volumes into combined sewer systems? (b) Does the operation of such installations affect local groundwater levels?

To answer these questions, we evaluated the hydrologic effects of a bioretention cell that was installed in early 2015 in the city of Cleveland, Ohio. Using a numerical simulation created within the program HYDRUS-2D/3D (Simunek & Sejna, 2011) that was supported and calibrated by observational monitoring data, we explored how bioretention cell design variables and local soil properties affect system performance and hydrological responses in terms of stormwater exfiltration and groundwater mounding dynamics. This information is highly relevant to municipalities and agencies as they seek to make strategic investments in GI that will reduce stormwater loads without causing unintended effects (e.g., basement flooding).

2 | METHODS

2.1 | Site and instrumentation

The studied bioretention cell was built on a vacant lot on E. 75th Street in the Slavic Village community of Cleveland, Ohio (Figure 1). The basin contained two media layers: (a) an engineered sandy loam soil amended with compost to form a biosoil, and (b) an aggregate base layer designed for stormwater storage. The cell had approximate dimensions of 5 × 9.6 m (48 m^2) and was connected to E. 75th Street via a curb-cut inlet (Figure S1). Surface runoff came from a surrounding impervious area of approximately 1,000 m^2, which was composed

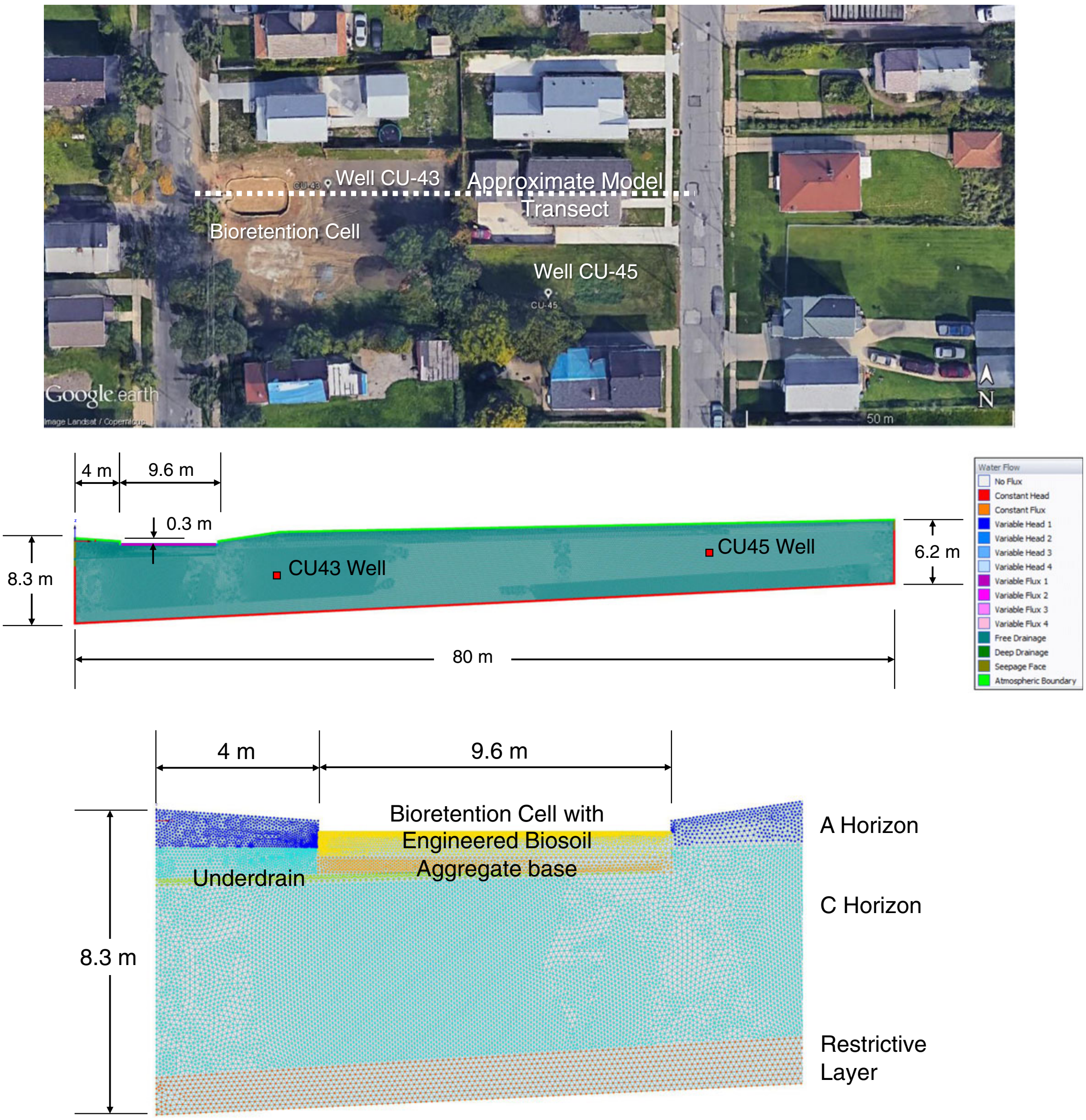

FIGURE 1 (top) Overhead view of site, showing approximate model domain and nearby groundwater monitoring wells CU-43 and CU-45. The studied bioretention basin can be seen under construction near the upper left corner of the approximate model domain; approximate transect used for the model are shown by the dashed line. (middle) Two-dimensional (x-z) transect created using HYDRUS-2D/3D, indicating domain dimensions, locations of observation nodes corresponding to two local monitoring wells (CU-43 and CU-45), and boundary conditions (as indicated by the colours on the outside nodes). (bottom) Distribution of soil/media layers within the HYDRUS-2D/3D model domain

mostly of transportation surfaces, rooftops, and sidewalks. Sheet flow from the residential areas around the basin was considered negligible.

The bioretention cell was designed to collect and infiltrate all water volume that entered the through the inlet, any runoff from surrounding permeable area, and direct rainfall onto the bioretention basin surface. An overflow drain was installed (diameter 0.15 m; inlet elevation 0.15 m above the bioretention cell surface) to collect excess ponded water volumes. A perforated underdrain pipe (0.15 m diameter) network was also installed below the rooting zone with the main lateral running through the centre of the garden to collect any excess drainage water beneath the aggregate base layer. The overflow and underdrain systems were connected together and plumbed to the combined sewer system (Figure S2). Thus, stormwater collected by either pipe contributed to direct return flow to the sewer network, though this flow would typically be delayed by some amount of time.

An instrumented weir (Figure S1) measured inflow into the bioretention cell on 2-min intervals; these data were aggregated to hourly volumes, which were then divided by the cross-sectional area of the basin (48 m^2) to estimate the equivalent flux of water. Inlet flow rate was recorded between 14 May 2015 and 31 October 2016. Outflow from the bioretention cell to the combined sewer system was monitored beginning on 23 March 2016 via a nonvented pressure transducer (15-min recording interval). This sensor was located at the juncture between the overflow and underdrain pipes (Figure S2) and enabled recording of stage height in the outfall system but not discharge. Therefore, we were limited to measuring event timing and cumulative outflow duration.

Twenty piezometers were installed throughout the study area and were outfitted with logging pressure transducers (SWS mini-Diver; Delft, Netherlands) to measure hourly water level. Groundwater

TABLE 1 Hydraulic properties calculated for the 75th Street South Rain Garden site, based on interpretations of soil cores and infiltration tests conducted near the site. Values are shown as arithmetic mean ± one standard deviation

	θ_r	θ_s	α (m^{-1})	n	K_s (m hr^{-1})
A horizon	0.049 ± 0.0098	0.39 ± 0.042	1.9 ± 0.95	1.47 ± 0.058	0.012 ± 0.0082
C horizon	0.051 ± 0.012	0.40 ± 0.023	1.9 ± 0.91	1.48 ± 0.12	0.0013 ± 0.0017

elevation data for the wells closest to the bioretention cell (CU-43 and CU-45; Figure 1) were used for model calibration/validation. Data from monitoring wells CU-30, CU-37, and CU-40 were used to determine regional groundwater levels (Figure S3). Fourteen time-domain reflectometer-type soil moisture sensors (Campbell Scientific; Logan, UT) were installed in multidepth nests around the cell, with 10 sensors placed within the biosoil layer and the other four placed in the anthropogenic or gleyic (reduced) native C horizons that underlay and surround the basin.

Hourly precipitation (P_O) and potential evapotranspiration (ET_O) rates were determined using data from two nearby weather stations, each located within 300 m of the site (ET107; Campbell Sci., Logan, UT). Warm-season precipitation was collected with a 0.025 cm resolution tipping bucket rain gage. Relative humidity, wind speed and direction, solar radiation, and air temperature were also measured and synthesized with rain catch within the ET107 operating system to generate hourly reference evapotranspiration (ET_O), using the ASCE Standardized Reference Evapotranspiration equation (Penman-Monteith method). Precipitation and ET_O data can be accessed at: http://waterdata.usgs.gov/oh/nwis/uv?site_no=412743081381400.

Soil cores were collected at 20 locations within a 300 m radius of the site. Samples were assessed for horizon location and thickness; texture (% sand, silt, and clay) of each horizon; colour (as Munsell hue, value, and chroma); redox features; pH; P, K, Mg, Ca and cation exchange capacity (using a Mehlich3 extraction); rock fragments; % C and % N; and Zn, Cu, and S. At the same locations, infiltration tests were conducted using mini-disk tension infiltrometers (Decagon Devices; Pullman, WA). Unsaturated hydraulic conductivity (i.e., K(−2 cm); n = 4) was then determined from steady-state data following manufacturer recommendations. Borehole saturated hydraulic conductivity measurements were also collected at each site using Amoozemeter-type compact, constant-head permeametres. Data were processed as per Amoozegar (1989), with application of the Glover solution.

2.2 | Numerical model

To integrate the observed hydrologic data, we constructed a numerical simulation of the site using HYDRUS-2D/3D (Version 2.05). Using the two-dimensional general option, we simulated a vertical transect (x–z plane) through the middle of the bioretention cell (Figure 1); the model domain was 80 m wide with a height that varied from 6.2 (on the far edge adjacent to E 76th Street) to 8.3 m (on the end corresponding to E 75th Street). Two periods were modelled: preinstall, from 1 September 2013 to 31 December 2014 (487 days), and postinstall, from 1 January 2015 to 9 August 2016 (586 days). Hourly time steps were used. Based on the soil core data, the native soil was represented by three layers: (a) the upper A horizon, (b) the parent material (C horizon), and (c) a restrictive layer composed of fractured bedrock material. The A horizon was approximately 1 m thick, whereas the C horizon was 3–6 m thick (Figure 1). The restrictive layer thickness varied from 1 (beneath E 75th Street) to 2.1 m (beneath E 76th Street). For the postinstall period, the bioretention cell was modelled as having a width of 9.6 m and was represented by a two layers: (a) an engineered biosoil top layer with 0.7 m thickness and (b) a 0.4 m thick aggregate base. The underdrain system was represented by a permeable layer that extended from beneath the bioretention cell to the edge of the domain corresponding to E 75th Street (Figure 1).

Soil core textural data (Table 1) were input into the neural network prediction tool of HYDRUS (Schaap, 1999) to estimate van Genuchten water retention parameters θ_r (residual water content), θ_s (saturated water content), and α and n (water retention curve shape parameters; Table 2). Saturated hydraulic conductivity (K_s) of the A and C horizons were constrained using the in situ infiltration tests. For the A horizon, the mini-disk tension infiltration data were used, whereas for the C horizon, the borehole infiltration data were used. The mean K_s for the A horizon was calculated as 0.012 ± 0.0082 m h^{-1}, and the mean K_s for the C horizon was calculated as 0.0013 ± 0.0017 m h^{-1} (Table 1). Based on subsequent calibration, the restrictive layer was set as $K_s = 8 \times 10^{-5}$ m h^{-1}. The hydraulic properties of the cell materials (i.e., the engineered biosoil, aggregate base, and underdrain) were assumed based on reasonable values for coarse-textured soil, with the biosoil K_s subsequently adjusted via calibration (Table 2).

In the preinstall period, the entire upper surface was given an atmospheric boundary condition. To convert ET_O calculated from the weather stations into actual evapotranspiration for input into the model, we used a scaling "crop" coefficient (k_c), such that $ET = k_c * ET_O$. k_c was set equal to 0.85, which is representative of a typical cool-season turfgrass stand (Romero & Dukes, 2016). We also used an empirical scaling factor (k_p) to convert observed precipitation (P_O) into a model input (P), such that $P = k_p * P_O$. k_p was set equal to 0.75 to account for precipitation losses due to vegetation interception (Corbett & Crouse, 1968) and overland flow from impervious or compacted areas. For the period between 12 June and 9 July 2015, which was characterized by a number of long duration storms, the

TABLE 2 Hydraulic properties used in the HYDRUS-2D/3D model

	θ_r	θ_s	α (m^{-1})	n	K_s (m hr^{-1})
A horizon	0.05	0.39	1.1	1.47	0.012
C horizon	0.05	0.40	0.19	1.48	0.0013
Restrictive layer	0.05	0.30	0.05	1.5	0.0001
Drain tile	0	0.95	2.5	1.6	0.8
Biosoil	0.01	0.41	2.35	1.6	0.08
Aggregates	0	0.28	2.1	1.6	0.2

maximum hourly rainfall rate was set to 0.003 m h^{-1} to ensure model convergence.

For the postinstallation period, the bioretention cell surface was modelled as having a variable flux boundary condition (Figure 1). The flux into the cell (q_{in}) was calculated as:

$$q_{in} = \mathrm{ET}-Q_{in}/A_{BC}, \tag{1}$$

where Q_{in} is the measured volumetric flow rate into the bioretention cell (in m^3 h^{-1}), A_{BC} is the area of the bioretention cell (48 m^2), and ET is the evapotranspiration rate (in m h^{-1}).

Between 1 January and 14 May 2015, the inlet weir was not instrumented. To provide estimates of inflow (Q_{in}) for this period, we used a calibrated SWMM model. The entire drainage area to the cell was approximately 3,600 m^2, of which 1,000 m^2 (27%) was impervious area. With this spatial information, the SWMM model was initially arranged and then calibrated using the measured 5-min rainfall and 2-min flow data. From the calibration, the directly connected impervious area of the site was estimated as 550 m^2 (15% of the drainage area). A comparison between the measured and SWMM-derived inflow rates showed that the SWMM model had good predictive value (R^2 = 0.76; Figure S6), though the SWMM model underpredicted inflow from large events. There were no large precipitation events recorded during this time period (one storm with a maximum hourly rate of 0.007 m h^{-1}; all other precipitation rates ≤0.005 m h^{-1}), making it feasible that the SWMM model input was sufficiently accurate. For the remainder of the model period (15 May 2015 to 9 August 2016), the measured inflow record was used to drive the bioretention cell boundary condition.

For both periods (preinstallation and postinstallation), the bottom domain boundary was modelled using a constant head of h = 5 m. The side boundaries had hydrostatic constant head boundaries for the lower portion, ranging from h = 5 m at the bottom to h = 0 m at the top, whereas nodes above the water table surface had the seepage face condition. Nodes corresponding to the subdrain outlet had a free drainage boundary condition (Figure 1). Observation nodes were placed to represent pressure transducer locations in wells CU-43 and CU-45, for comparison of measured and modelled pressure head values. Other nodes were used to generate time series for soil moisture in the bioretention cell biosoil and native soil A horizon (Figure S5).

HYDRUS tracked and quantified the fluxes into and out of the domain for every time step and on a cumulative basis. We used the cumulative output to quantify the water mass balance, as these data are more accurate than the fluxes (which are generated using average values). Because a two-dimensional model was used, cumulative volumes are presented in terms of cubic metre water per metre of domain (to account for the third dimension that was not modelled). We multiplied the cumulative inflow predicted by the model (in m^3 m^{-1}) by the approximate width of the bioretention basin (5 m) to get infiltrated volume ("Inflow") in terms of volume (m^3). This approach allowed for direct comparison with the inflow volumes measured at the site.

2.3 | Model parameter sensitivity and calibration

Wherever possible, we used model parameters that were estimated via physical measurements (e.g., infiltration testing and field soil assessment) in an effort to reduce model uncertainty. However, the model required further calibration to better match, for example, water table fluctuations in the surrounding soil. To this end, we used four tuning parameters that were associated with hydraulic properties of the model: K_s of the biosoil layer, K_s of the lowest restrictive soil layer, α of the A horizon, and α of the C horizon. These hydraulic parameters were calibrated by comparing measured and modelled water table elevations for CU-43 and CU-45 between 1 November 2015 and 9 August 2016. Specific criteria used to determine goodness of fit were (a) root mean square deviation (RMSD) between measured and modelled water table elevations and (b) timing and magnitude of water table rise and recession in response to precipitation events.

We also performed a sensitivity analysis on the model by adjusting K_s and α for the engineered biosoil (i.e., the top bioretention cell layer) and for the surrounding A and C horizons (Table 3). The water retention parameter n was also adjusted for the A horizon but showed little effect on the model response and so was excluded from further analysis. In total, a 170-day (4,084 hr) period, representing 1 January 2015 to 20 June 2015, was simulated for each parameter combination. The corresponding model response was then quantified using six metrics: (a) RMSD between observed and modelled water table for monitoring wells CU-43 and CU-45; (b) infiltration through the bioretention cell surface; (c) drainage flux through the free drainage boundary condition that represented the underdrain outlet; (d) mean water level in wells CU-43 and CU-45; (e) range of water levels in wells CU-43 and CU-45 (i.e., the difference between the maximum and minimum water levels recorded during the model period); and (f) water table variation in wells CU-43 and CU-45 on 28 May 2015, a date that is considered to be representative of typical diurnal variability. Note that the "original" values chosen for α differ from those used in the final model due to the subsequent calibration.

The calibrated HYDRUS model was used to analyze a scenario in which the bioretention cell had not been installed (i.e., with only native soil and no stormwater volume input from the street, called hereafter the "No Bioretention" scenario). The modelled hydrological responses of the as-built "With Bioretention" and hypothetical No Bioretention scenarios were quantified by comparing cumulative mass balances. Specific mass balance components included: infiltration through the

TABLE 3 Hydraulic parameters used in the sensitivity analysis. α values have units of m^{-1} and K_s values all have units of m h^{-1}

	$\alpha_{original}$	α_1	α_2	α_3	α_4	$K_{s,original}$	K_{s1}	K_{s2}	K_{s3}	K_{s4}
A horizon	0.14	0.014	0.07	0.28	1.4	0.012	0.0012	0.024	0.12	0.12
Engineered biosoil	1.05	0.105	0.525	2.1	10.5	0.08	0.008	0.04	0.16	0.8
Relative magnitude	1	0.1	0.5	2	10	1	0.1	0.5	2	10

bioretention cell surface (Inflow); infiltration and evaporation through the surface outside of the bioretention basin ("Atmosphere"); drainage through the underdrain ("Drainage"); drainage through seepage face nodes on the side boundaries ("Seepage"); fluxes through the constant head boundary on the bottom and lower sides of the domain ("Recharge"); and storage within the domain as determined from the residual term of the mass balance ("Storage"). Note that by definition the No Bioretention scenario did not include the Inflow and Drainage terms.

3 | RESULTS

3.1 | Inflow

The cumulative measured inflow into the bioretention cell (in m^3) was compared to the modelled inflow for the period from 14 May 2015–9 August 2016 (Figure 2). The model showed 505 m^3 of inflow into the bioretention cell, whereas the measured inflow volume was 892 m^3. The model therefore only accounted for 56% of the observed inflow. The discrepancy between the modelled and observed inflow volumes was likely attributable to the constrained pressure heads used on the variable flux model boundary condition. This option ensured model stability but also meant that during large inflow events (such as occurred 30 May–1 June 2015), the model domain infiltrated less water than actual. On the other hand, for other periods with lower stormwater inputs (e.g., 1 October–31 December 2015), the model closely approximated the measured infiltration volumes. Looking at the between 24 March and 9 August 2016, the total duration of warm-season inflow events was measured to be 221 hours (i.e., the cumulative amount of time in which inflow was measured).

3.2 | Outflow

A pressure transducer installed in the subsurface drainage system measured the initiation and duration of ponding within the underdrain system (though not drainage flux, due to the lack of a suitable rating curve). Between 24 March and 9 August 2016, the sensor recorded a total outflow duration of ~29 hr from 16 events with water levels >0.01 m (Figure 3). The model predicted 11 events with a drainage flux >0.01 $m^2\ h^{-1}$ during this same period. Note that "events" in both cases were defined to have occurred whenever the drainage flux or water level showed a local maximum (peak). The model and observations both indicated drainage on nine occasions, giving the model two "false positives" (that occurred before 20 April 2016) and seven "false negatives" (that all occurred after 20 April 2016). The bioretention cell surface showed some evidence of preferential flow during the summer of 2016, including subsidence above the outfall drain and associated cracks, which could have driven a non-equilibrium drainage process that was not captured by the model.

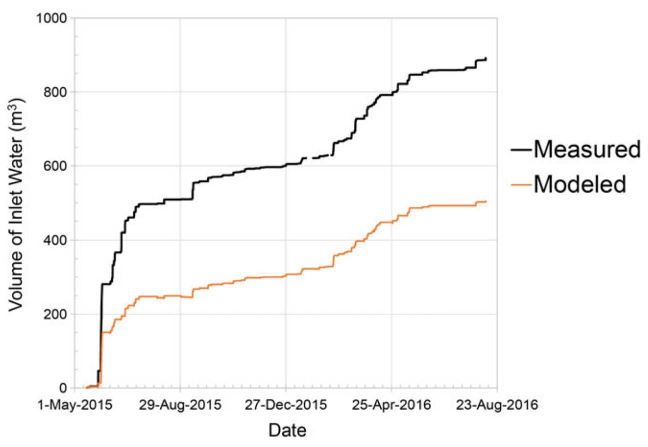

FIGURE 2 Cumulative stormwater inflow (in cubic metre) that was measured using an instrumented weir placed between the road and bioretention basin (black line) compared to the modelled infiltration volume into the basin (orange line)

3.3 | Surface ponding

The bioretention cell was also outfitted with a pressure transducer that measured surface ponding between 13 August 2015 and 9 August 2016. During this time, the bioretention cell had only six inflow events that caused measurable ponding (Figure 4), with three of those events persisting for longer than a single 5-min record. The longest duration ponded event occurred on 12 September 2015, in which the bioretention cell recorded >0.04 m of water for two 10-min periods that were separated by 1 hr. Five of the six ponding events were associated with inflows that peaked above 0.15 m h^{-1} (7 $m^3\ h^{-1}$), with the sixth resulting from a low-intensity, multi-day event that occurred between 11 and 15 November 2015. These data therefore show that the bioretention cell ponded only for brief periods during the largest inflow events (i.e., inflow rates >0.15 m h^{-1}).

The model predicted ponding to occur at a similar frequency, with eight ponded events (Figure 4). Of those, five occurred at the same time as the model predicted ponding, whereas the other three occurred at times when ponding was not detected at the site. The model and observations agreed on the depth of ponding for two events and disagreed on three. For instance, the model predicted ~0.01 m of surface ponding on 29 July 2016, which was the largest

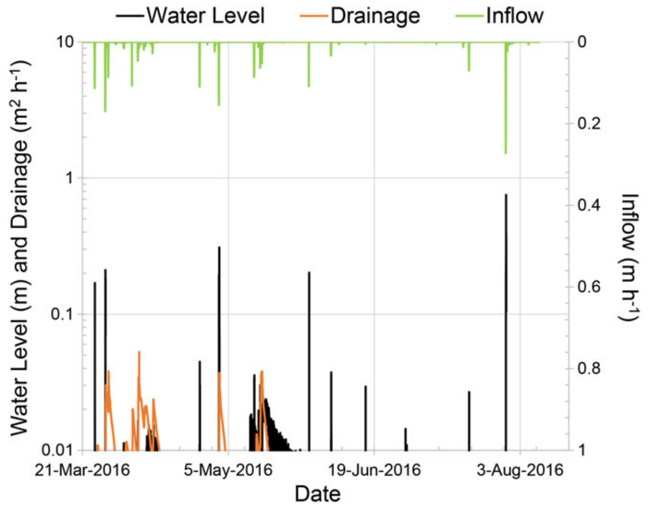

FIGURE 3 Comparison of the water level measured in the underdrain outflow system (black line) with modelled flux through the underdrain system (orange line). Measured stormwater inflow (green line) is shown at the top

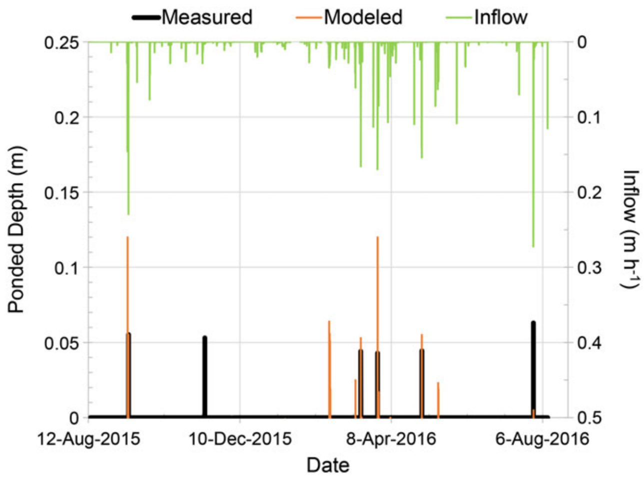

FIGURE 4 Comparison of observed (black lines) versus modelled (orange lines) ponding depths at the bioretention cell surface. Inflow (green lines) is indicated at the top

measured inflow and ponding event. The model predicted that two events caused ponded depths >0.1 m, whereas the greatest observed ponding depth was ~0.06 m. The bioengineered soil surface was built to be approximately 0.3 m lower in elevation than the surrounding soil and also included an overflow pipe that prevented ponding depths greater than ~0.15 m (though the measured water levels suggested water did not pond sufficiently high to drain through the overflow). Taken together, the model and measurements indicated that the majority of stormwater inflow events occurred at rates that were less than the hydraulic conductivity of the bioretention basin material (i.e., $Q_{in}/A_{BC} < K_s$). This result implies that the cell was capable of infiltrating large volumes of street stormwater without risk of overtopping and causing flooding in adjacent areas.

3.4 | Groundwater elevations

The numerical model captured many aspects of the overall groundwater dynamics, though the predicted water levels occasionally differed from the observed water levels in wells CU-43 and CU-45 (Figures 5a). For the period before bioretention cell installation (i.e., 30 September 2013–31 December 2014), the model captured the timing and magnitude of groundwater responses to precipitation events in well CU-43. The modelled water level in well CU-45 was substantially higher than was observed for the period 30 September 2013 to 15 May 2014 (Figure 5b), for reasons that remain unclear. The RMSD between modelled and measured water levels in 2014 was better for well CU-43 (0.045 m) compared to well CU-45 (0.14 m). However, some of the large variations seen in the observational data may be attributed to the wells gaining proper hydraulic connection to surrounding soils in the period after initial installation (which occurred

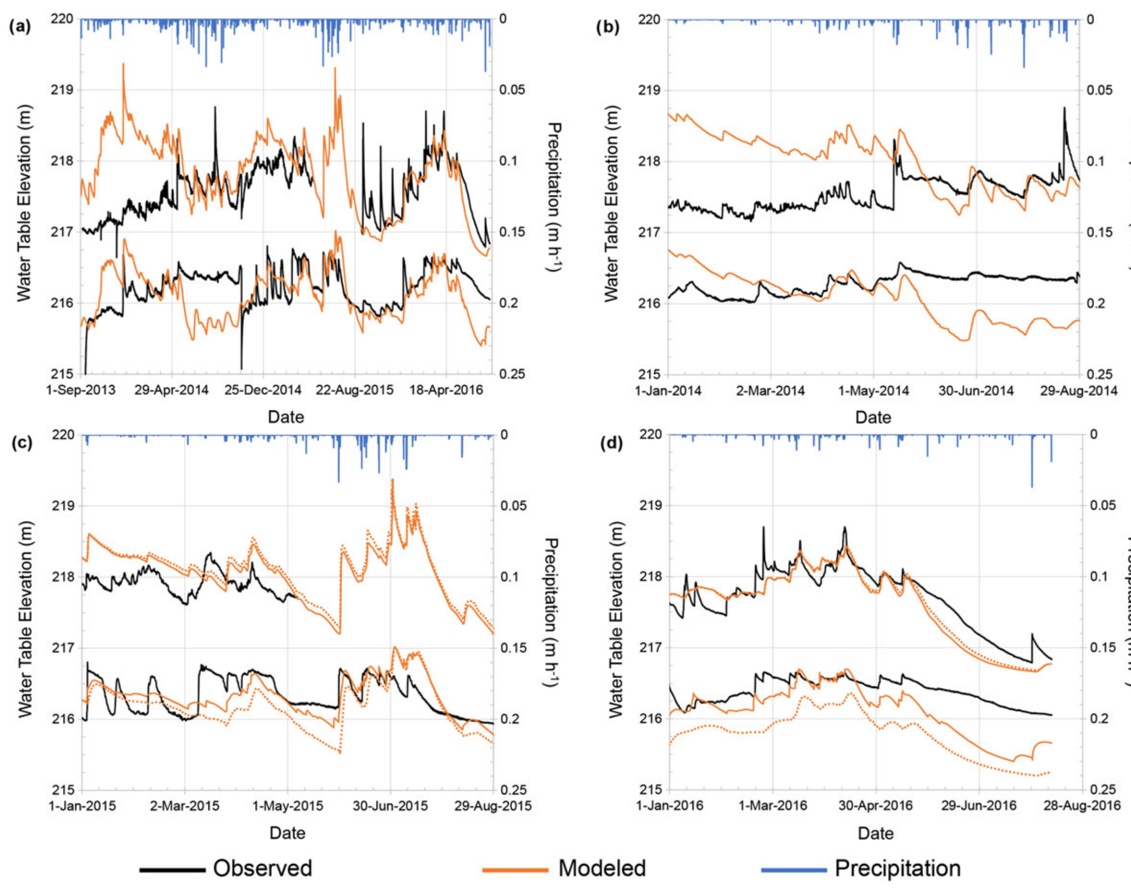

FIGURE 5 Observed versus modelled water table elevations (above NAVD88) for groundwater wells CU-43 (lower lines) and CU-45 (upper lines), with hourly observed precipitation indicated at the top. In (c) and (d), solid orange lines show the "With Bioretention" water levels, whereas the dotted orange lines show the "No Bioretention" water levels. Results are shown for (a) the entire model period from 1 September 2013 to 9 August 2016; (b) 1 January to 29 August 2014, before the bioretention cell was installed; (c) 1 January to 29 August 2015, after the bioretention cell was installed; and d) 1 January to 28 August 2016

in August/September 2013), as variability in water surface measurements were higher initially than for subsequent events.

The 2 years of bioretention cell operation (2015 and 2016) provided a range in weather conditions. Year 2015 was characterized by a number of large springtime storms, in which the water table elevations cycled corresponding to inflows (Figure 5c). The model captured those dynamics well, with an RMSD of 0.0030 m in well CU-43 and 0.013 m in well CU-45 for the year 2015. In contrast, 2016 had regular, low intensity precipitation events, with a single storm in July that exceeded 0.02 m h^{-1}. During this period, the model matched well during the spring and early summer, but during the summer, the model predicated a relatively large decline in the water table at CU-43 relative to the observed values (Figure 5d). The total RMSD for measured and modelled water levels in CU-43 was 0.020 m for 2016. CU-45, on the other hand, had very close agreement between measured and modelled water levels throughout 2016, with an RMSD of 0.0027 m. These RMSD values were within the range of accuracy listed for the mini-divers used in the study (0.005 m). For the entire 3-year study period, the water level RMSD values were 0.026 m for CU-43 and 0.12 m for CU-45, suggesting an overall good match between the model and observations. For the postinstall period, the RMSD values were 0.0070 m for CU-43 and 0.0071 m for CU-45, which are similar to the accuracy of the level loggers used in the study.

The simulation in which the bioretention cell was not included (No Bioretention) showed different water table elevations compared to the With Bioretention scenario. In the well nearest to the bioretention cell (CU-43), the water table was 0.2–0.5 m lower in elevation in the No Bioretention scenario (Figure 5c,d). In well CU-45, the No Bioretention simulation showed slightly higher water levels than the With Bioretention run, with differences up to 0.1 m. Therefore, the model suggests that the bioretention cell may have moderated the up-gradient slope of the water table, possibly due to increased water mounding around the bioretention basin. The visual output from the model also revealed that this mounding was localized to a lateral distance of 10–20 m away from the cell (Figures S9 and S10).

3.5 | Soil water content

As a final check on model performance, we compared observed and modelled soil water content for the bioretention cell rooting zone (biosoil) and native soils during a 2-week period (from ~5 cm depths). The model captured general wetting and drainage dynamics, with a RMSD of 0.096 $m^3\ m^{-3}$ for the bioretention cell biosoil and 0.034 $m^3\ m^{-3}$ for the native A horizon soil (Figure 6). During and for 3 days following a large storm on 29 July 2016, the model accurately predicted water content in the A horizon, though it overpredicted water retention in this material for the latter part of the recession period. The model predicted consistently higher water content values for the biosoil material compared to observed values and also showed greater sensitivity to small rainfall events (e.g., on 30 July and 5 August 2016). This latter result may provide another indication of preferential flow through the bioretention cell, by which incoming stormwater was shunted to the storage layer or moved outside of the basin along subsurface channels (e.g., structural cracks, uncharacterized sand

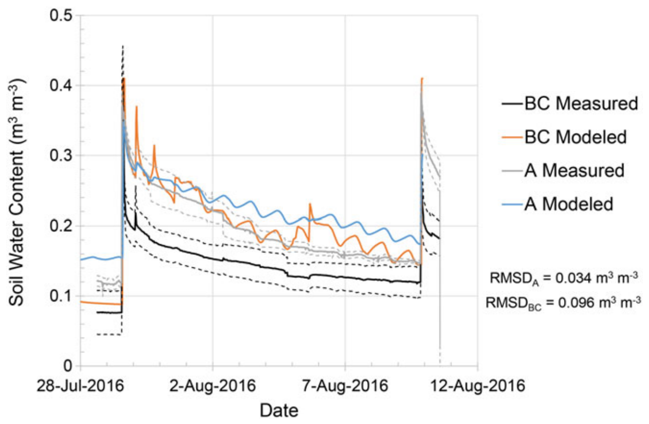

FIGURE 6 Measured versus modelled volumetric soil water contents at a 5 cm depth for the bioretention cell biosoil layer (RG; yellow and black lines) and surrounding A horizon of the native soil (A; blue and gray lines). Dashed lines indicate 95% confidence intervals for the measured water contents

lenses from construction). The model more accurately predicted water contents in the biosoil layer after multi-day drying periods (e.g., 28–29 July), suggesting that the hydraulic properties used in the model were appropriate.

3.6 | Mass balance of the bioretention cell

We next used the calibrated HYDRUS model to examine water mass balance for the bioretention cell. In this analysis, we compared the model for the site with the bioretention cell as it was built and operated with a second scenario in which the bioretention cell had not been installed (i.e., only native soil; no additional stormwater input). In the calibrated "as-built" model (With Bioretention – Figure 7a), the largest input came from infiltration via the bioretention basin surface, with a cumulative volume of 120 $m^3\ m^{-1}$ between 1 January 2015 and 9 August 2016. A portion of this infiltrating water was then removed via drainage through the underdrain (cumulative output of 45 $m^3\ m^{-1}$). Water also drained from the bottom and sides of the domain, with a cumulative output of 27 $m^3\ m^{-1}$ through the constant head boundary (Recharge) and 7.3 $m^3\ m^{-1}$ through the seepage face boundary (Seepage). The atmospheric boundary (Atmosphere) acted as a net output, with 10 $m^3\ m^{-1}$ more water leaving the domain via evapotranspiration as compared to what entered the domain via precipitation. Domain storage underwent a series of spikes and recessions in response to precipitation but overall increased due to bioretention cell operation by ~30 $m^3\ m^{-1}$. Note that this storage value represents a volumetric water increase of 0.052 (5.2%) based on the total domain volume of 575 $m^3\ m^{-1}$. When the model was run without the bioretention cell (No Bioretention – Figure 7b), the storage term decreased as water drained through lower boundaries, with total decrease of 14 $m^3\ m^{-1}$ (0.025 $m^3\ m^{-3}$ or 2.5%). The atmospheric demand for water was identical to that of the With Bioretention scenario, with an overall cumulative loss of ~10 $m^3\ m^{-1}$. The seepage flux nodes had a negligible contribution in this scenario.

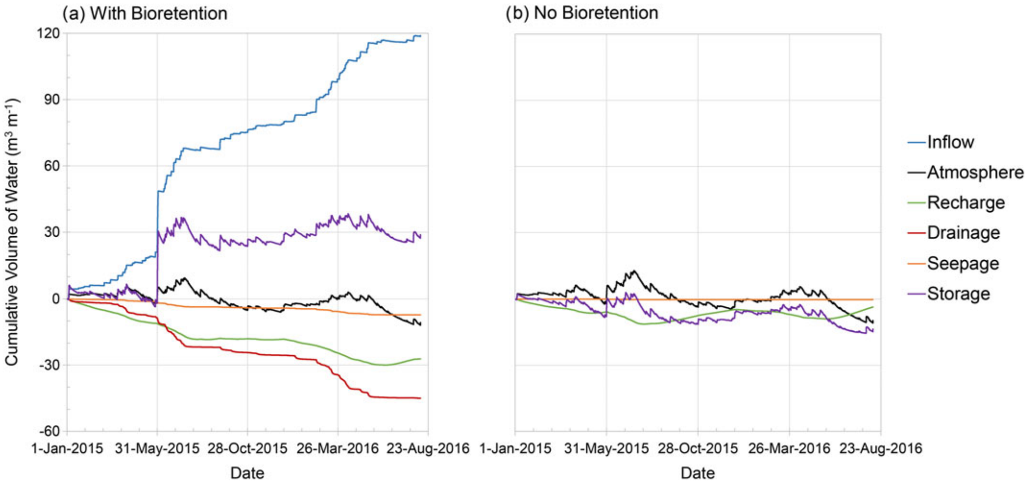

FIGURE 7 Cumulative water balance on the model domain for two scenarios: (a) "With Bioretention", which considers the bioretention cell under normal operation; and (b) "No Bioretention", where the domain is modelled without the bioretention basin installed (i.e., native soil and no additional stormwater input). Positive values indicate water entering the domain, whereas negative values indicate water leaving. Increases in soil water storage are shown as positive values; decreases are shown as negative

3.7 | Model sensitivity

We performed a sensitivity analysis to assess how different soil hydraulic properties (e.g., K_s and α) affected bioretention cell performance. Water levels in the nearest monitoring well (CU-43) were most sensitive to the K_s and α of the biosoil; infiltration flux into the bioretention cell was also strongly affected by K_s of the biosoil (Figure 8). Specifically, higher biosoil K_s values caused the basin to infiltrate more water, which resulted in increased error between observed and modelled water table elevations, whereas lower biosoil K_s values reduced infiltration, which dampened water level variations in the surrounding soils and slightly decreased the mean water table elevations (Table 4; also Figure S10).

The α parameter, in particular, acted as a dominant control on the magnitude of daily and seasonal fluctuations in water table elevations, with smaller α values associated with greater event-based variations but lower seasonal variations. The model showed some sensitivity to α of the A horizon, with higher α values associated with lower RMSD values for CU-43 and CU-45. The model had similar sensitivity to α of the C horizon (data not shown), so the overall soil profile behaved consistently in this regard. This effect was likely due to small α values being associated with a gradual, smooth slope of the water retention curve and also with large capillary rise (Raats & Gardner, 1971). This larger matric potential (large capillary rise) also meant that near-surface soil water content showed extreme sensitivity to the choice of α for the A horizon and biosoil material, with low α values causing the soil water content to become essentially constant throughout the run, as it was in effect replenished via continual upward wicking of water from the groundwater table due to capillarity.

4 | DISCUSSION

This study had two main purposes: (a) evaluate the ability of a street-side bioretention cell installed with an underdrain system to reduce stormwater flows into a combined sewer system and (b) determine the magnitude and extent of any groundwater changes resulting from any stormwater that exfiltrated from the system. The mass balance information provided by the model, augmented by observational records collected at the site, allowed us to explore both of these

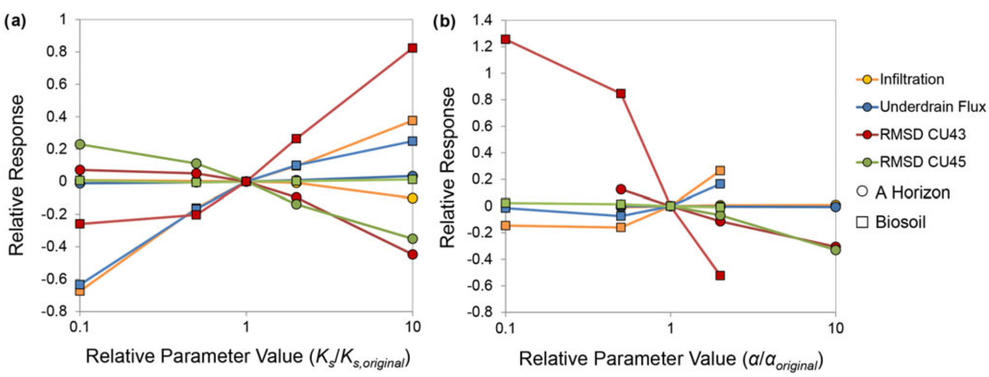

FIGURE 8 Results of the sensitivity analysis, where the model sensitivity to relative changes in (a) saturated hydraulic conductivity (K_s) and (b) van Genuchten parameter α was quantified. Four response metrics are presented: infiltration through the bioretention cell surface; flux through the subsurface underdrain beneath the basin; and root mean square deviation (RMSD) between the observed and modelled water table elevations in wells CU-43 and CU-45. Missing values indicate parameter combinations where the model did not converge

TABLE 4 Results of the sensitivity analysis for various parameter values of van Genuchten α and saturated hydraulic conductivity K_s for the A horizon of the natural soil and the engineered biosoil within the bioretention cell. The responses are measured as mean water levels, level ranges (i.e., difference between maximum and minimum water level), and diurnal variation (i.e., maximum daily difference in water levels) for wells CU-43 and CU-45. All water levels are in meters

	Relative Magnitude	Mean level Well CU-43	Mean level Well CU-45	Level range Well CU-43	Level range Well CU-45	Diurnal change Well CU-45
A horizon: $\alpha_{original}$ = 0.14 m^{-1}; = $K_{s,original}$ = 0.012 m hr^{-1}						
$\alpha_{original}$	1	215.8	217.6	1.38	1.12	0.064
α_2	0.5	215.8	217.5	1.95	1.33	0.135
α_3	2	215.8	217.6	1.05	0.96	0.032
α_4	10	215.9	217.7	0.79	0.83	0.005
$K_{s,original}$	1	215.8	217.6	1.38	1.12	0.064
K_{s1}	0.1	215.8	217.5	1.24	1.11	0.018
K_{s2}	0.5	215.8	217.5	1.31	1.14	0.065
K_{s3}	2	215.9	217.6	1.51	1.08	0.062
K_{s4}	10	216.0	217.5	1.70	0.80	0.063
Biosoil: $\alpha_{original}$ = 1.05 m^{-1}; = $K_{s,original}$ = 0.08 m hr^{-1}						
$\alpha_{original}$	1	215.8	217.6	1.38	1.12	0.064
α_2	0.1	215.5	217.5	1.80	2.32	0.064
α_3	0.5	215.6	217.5	1.67	1.87	0.064
α_4	2	216.0	217.6	1.19	0.60	0.005
$K_{s,original}$	1	215.8	217.6	1.38	1.12	0.064
K_{s1}	0.1	215.9	217.6	0.94	0.82	0.064
K_{s2}	0.5	215.9	217.6	1.27	0.91	0.064
K_{s3}	2	215.7	217.6	1.50	1.37	0.064
K_{s4}	10	215.6	217.5	1.70	1.90	0.065
Observed values		216.4	217.6	0.83	1.68	0.04

themes in detail. For instance, the model predicted that less than 40% of the inflow into the bioretention cell was returned to the combined sewer system (i.e., the drainage term in Figure 7), whereas a nearly equal magnitude of inflow became stored as increased soil water (i.e., the storage term in Figure 7). Comparing the With and No Bioretention scenarios, operation of the bioretention system was predicted to have resulted in a net soil water storage increase of nearly 45 m^3 m^{-1} (Figure 7), which corresponded to a mean soil water content increase of ~8%. This increase in soil water storage translated to the local water table becoming elevated by up to 0.5 m. Still, this groundwater level increase was primarily observed in the nearby CU-43 well, with negligible effects seen at the more distant CU-45 well. Thus, it appears that changes in water table elevations caused by the bioretention basin operation were minor and localized enough to not threaten other belowground infrastructure.

The modelled result that exfiltration from the bioretention cell reduced return flow volumes was supported by the observational data during low and moderate inflow events. For example, between 24 March and 9 August 2016, the total duration of warm-season inflow events was measured to be 221 hr, whereas the outflow duration during this period was roughly 29 hr (1/8 of total inflow duration). Much of the infiltrated stormwater therefore either exfiltrated from the bioretention cell or drained through the subsurface system slowly enough so as not to induce ponding in the drainage standpipe. However, there is an important caveat to these results: the model did not capture total observed inflow, with the discrepancy primarily driven by large inflow events (where the model predicted less inflow than observed). Observed water levels in the underdrain suggested that the drainage system became active during high inflow events, so it is likely that much of the stormwater during large events had a short residence time in the basin before entering the wastewater collection system as return flow. Thus, although underdrains may be useful in preventing surface ponding and excess groundwater mounding, they may also limit the effectiveness of infiltration systems in reducing stormwater volume during high inflow events (a finding also reported by Jarden et al. [2016] for a nearby region of northeastern Ohio). Large inflow events are often the most problematic in terms of combined sewer overflow incidence and treatment costs; as a result, agencies looking to install retrofit infiltration systems, as a way to reduce stormwater volumes in combined systems, may want to explore alternative methods or designs for underdrain systems. For example, drainage systems with high invert elevations (and thus greater internal water storage) may exhibit increased exfiltration and decrease discharge to storm systems compared to down-sloping drains (Brown & Hunt, 2011; Winston et al., 2016). However, care should be taken in such installations that the level of groundwater mounding is not increased enough to cause problems such as basement flooding.

4.1 | Model uncertainty and limitations

HYDRUS-2D/3D is a robust, physically-based model that numerically solves the Richards Equation (thus combining continuity with Darcy-Buckingham flow); nonetheless, it has various sources of uncertainty. One source of error (and uncertainty) is that which occurs when the model measures the water mass balance over the entire domain. This error is typically related to the node spacing, so we used node spacing of 0.05 m in the vicinity of the bioretention cell, and as a result, had overall mass balance errors of <1% for much of the run. It should be noted, however, that rainy periods with large inflow events (such as occurred in June–July 2015) were associated with mass balance errors up to 70% (in addition to the aforementioned underpredictions of inflow). Avoiding such errors would likely require running the model on smaller time and spatial resolutions, which could pose challenges in terms of both observational data and computational requirements.

Another source of uncertainty is the soil hydraulic parameters and their spatial variability. Moreover, we used mean sand, silt, and clay percentages as inputs into the ROSETTA pedotransfer functions to estimate the van Genuchten water retention parameters, which is associated with high uncertainty due to the necessarily limited sample set of disturbed cores used to generate the original regression relationships (Schaap, Leij, & van Genuchten, 1998). We also assumed uniform hydraulic parameters for each layer, even though in reality such properties often have wide spatial distributions (e.g., saturated hydraulic conductivity typically follows a log-normal distribution) within a single material. Our measured data reflect this variability, as K_s measured via infiltration testing for the A and C horizons showed standard deviation values that were equal in magnitude to the mean (Table 1).

The boundary conditions also caused uncertainty. For example, the study site is underlain by a relatively shallow restrictive layer, which, combined with the rolling surface topography, leads to a sloping regional water table. Analysis of groundwater levels along a roughly east to west transect revealed that the water table surface decreased by more than 10 m over a distance of approximately 320 m, giving a slope of more than 3% (Figure S3). Replicating the sloping water table in HYDRUS required the use of a constant head boundary condition, which did not account for any lateral subsurface flow or large-scale groundwater fluctuations that might have occurred at the site.

We created and explored a three-dimensional model of the site, but ultimately, this model lacked sufficient numerical stability to make it useful. At the same time, the two-dimensional model was sufficient to simulate most of the site features and processes of interest, allowing us to simulate the site slope, different soil layers, underdrain system, and approximate locations of sensors such as the groundwater monitoring pressure transducers and soil water content sensors. Still, geometric limitations of the two-dimensional model likely affected the partitioning of water within the bioretention cell. For instance, the two-dimensional domain gave the underdrain system an areal contribution that far exceeded that of the real (0.15-m diameter) pipe, such that the model effectively considered the underdrain to exist beneath the entire nonsimulated dimension of the bioretention cell. The model also likely underpredicted percolation from the basin into the native soil, as the effective perimeter of the simulated bioretention cell was much smaller than in reality. Infiltration from structures such as recharge basins and unlined wetlands has been shown to vary as a function of the perimeter to area ratio, with higher relative perimeters associated with greater infiltration (Petrides, Stewart, Bower, Cuenca, & Wolcott, 2014; Stewart, Moreno, & Selker, 2015). Together, these factors may have led the model to overpredict subsurface drainage via the underdrain system and underpredict exfiltration and groundwater mounding, thus increasing model uncertainty. These factors may also help to explain why the model predicted outflow from the subsurface drainage system to persist for much longer periods of time than were measured at the site (Figure 3).

5 | CONCLUSIONS

Installation of GI, such as bioretention basins, is used to curtail stormwater peak flows in urban areas and, in some instances, encourage groundwater recharge. In this study, we simulated the hydrology of a small-scale unlined bioretention cell using a HYDRUS-2D/3D numerical model that was augmented and calibrated by observational data from various sensors installed at the site. The final model was able to capture much of the groundwater dynamics that occurred at the site, including how water mounding and movement may have been altered by installation of the bioretention system. Comparison between the calibrated model and a version that simulated the same domain without the bioretention basin showed that stormwater infiltration altered the water mass balance and increased water storage within the subsurface. Thus, the model confirmed that the bioretention cell system acted to buffer and reduce stormwater flows that would otherwise be associated with potential flooding or water quality concerns. However, the model was not able to fully capture large inflow events; based on observational data from the site, such events may have been associated with the greatest and most rapid return flows into the combined sewer system. As a result, the effectiveness of bioretention installation may become reduced as inflow volumes and rates increase.

The model was also used to examine the sensitivity to key parameters, including saturated hydraulic conductivity and the water retention shape parameter α, for soil layers within and around the bioretention cell. The model showed high sensitivity to the properties of the basin biosoil, as this material controlled the ability of the bioretention cell to infiltrate water into the system, while also regulating the amount of groundwater mounding that occurred within the surrounding soil. The model response was also highly sensitive to α, as that parameter was seen to control the magnitude and frequency of groundwater elevation changes in response to rainfall events. α also strongly influenced the near-surface soil water content values, due to capillary connections that persisted between the phreatic and soil surfaces when small α values were tested.

Overall, the bioretention installation analyzed in this study provided an ideal test case, supported by a robust observational dataset, to understand local effects on hydrology. Specifically, this study provided new insight into how bioretention system operation activated and drove a new groundwater dynamic in the surrounding subsurface, a finding that has not previously been uncovered in such detail. The study also suggested that the stormwater infiltration system was most effective during small and moderate inflow events, but the presence of an underdrain system may have limited its utility during large inflow events. The study showed how field data and modelling techniques can be used to represent GI functions at the landscape scale and can anticipate and constrain design limitations and benefits. These results can in turn be used to inform future design and site selection considerations for infiltration-type GI installations.

ACKNOWLEDGMENTS

This study would not have been possible without the engagement of the Slavic Village Community Development Corporation and the Cuyahoga County Land Reutilization Corporation, Cleveland Botanical Garden, and Northeast Ohio Regional Sewer District (NEORSD). Monitoring was conducted under an interagency agreement between USEPA-ORD and the USGS Michigan-Ohio Water Sciences Center. The bioretention cell was constructed by NEORSD. Additional support came from the Virginia Agricultural Experiment Station and the Hatch Program of the National Institute of Food and Agriculture, U.S. Department of Agriculture. The views expressed in this presentation are those of the authors and do not necessarily represent the views or policies of the U.S. Environmental Protection Agency or the U.S. Geological Survey.

ORCID

Ryan D. Stewart http://orcid.org/0000-0002-9700-0351
Joong Gwang Lee http://orcid.org/0000-0003-4730-3466
William D. Shuster http://orcid.org/0000-0001-7688-0110
Robert A. Darner http://orcid.org/0000-0003-1333-8265

REFERENCES

Abi Aad, M. P., Suidan, M. T., & Shuster, W. D. (2009). Modeling techniques of best management practices: Rain barrels and rain gardens using EPA SWMM-5. *Journal of Hydrologic Engineering*, *15*, 434–443.

Ahiablame, L., & Shakya, R. (2016). Modeling flood reduction effects of low impact development at a watershed scale. *Journal of Environmental Management*, *171*, 81–91. https://doi.org/10.1016/j.jenvman.2016.01.036

Amoozegar, A. (1989). A compact constant-head permeameter for measuring saturated hydraulic conductivity of the vadose zone. *Soil Science Society of America Journal*, *53*, 1356–1361.

Avellaneda, P. M., Jefferson, A. J., Grieser, J. M., & Bush, S. A. (2017). Simulation of the cumulative hydrological response to green infrastructure. *Water Resources Research*, *53*, 3087–3101. https://doi.org/10.1002/2016wr019836

Bhaskar, A. S., Beesley, L., Burns, M. J., Fletcher, T. D., Hamel, P., Oldham, C. E., & Roy, A. H. (2016). Will it rise or will it fall? Managing the complex effects of urbanization on base flow. *Freshwater Science*, *35*, 293–310. https://doi.org/10.1086/685084

Bhaskar, A. S., Hogan, D. M., & Archfield, S. A. (2016). Urban base flow with low impact development. *Hydrological Processes: n/a-n/a*.. https://doi.org/10.1002/hyp.10808

Bhaskar, A. S., Welty, C., Maxwell, R. M., & Miller, A. J. (2015). Untangling the effects of urban development on subsurface storage in Baltimore. *Water Resources Research*, *51*, 1158–1181. https://doi.org/10.1002/2014wr016039

Brown, R., & Hunt, W. (2011). Underdrain configuration to enhance bioretention exfiltration to reduce pollutant loads. *Journal of Environmental Engineering*, *137*, 1082–1091.

Browne, D., Deletic, A., Mudd, G. M., & Fletcher, T. D. (2008). A new saturated/unsaturated model for stormwater infiltration systems. *Hydrological Processes*, *22*, 4838–4849.

Corbett, E. S., & Crouse, R. P. (1968). Rainfall interception by annual grass and chaparral... losses compared. Station Pacific Southwest Forest and Range Experiment Station (ed.) U.S.D.A. Forest Service, pp: 12.

Davis, A. P. (2008). Field performance of bioretention: Hydrology impacts. *Journal of Hydrologic Engineering*, *13*, 90–95.

Dietz, M. E. (2007). Low impact development practices: A review of current research and recommendations for future directions. *Water, Air, and Soil Pollution*, *186*, 351–363.

Dietz, M. E., & Clausen, J. C. (2005). A field evaluation of rain garden flow and pollutant treatment. *Water, Air, and Soil Pollution*, *167*, 123–138.

Dussaillant, A. R., Wu, C. H., & Potter, K. W. (2004). Richards equation model of a rain garden. *Journal of Hydrologic Engineering*, *9*, 219–225.

Eger, C. G., Chandler, D. G., & Driscoll, C. T. (2017). Hydrologic processes that govern stormwater infrastructure behavior. *Hydrological Processes*. https://doi.org/10.1002/hyp.11353

Endreny, T., & Collins, V. (2009). Implications of bioretention basin spatial arrangements on stormwater recharge and groundwater mounding. *Ecological Engineering*, *35*, 670–677.

Fanelli, R., Prestegaard, K., & Palmer, M. (2017). Evaluation of infiltration-based stormwater management to restore hydrological processes in urban headwater streams. *Hydrological Processes*, *31*, 3306–3319. https://doi.org/10.1002/hyp.11266

He, Z., & Davis, A. P. (2010). Process modeling of storm-water flow in a bioretention cell. *Journal of Irrigation and Drainage Engineering*, *137*, 121–131.

Jarden, K. M., Jefferson, A. J., & Grieser, J. M. (2016). Assessing the effects of catchment-scale urban green infrastructure retrofits on hydrograph characteristics. *Hydrological Processes*, *30*, 1536–1550. https://doi.org/10.1002/hyp.10736

Li, H., Sharkey, L. J., Hunt, W. F., & Davis, A. P. (2009). Mitigation of impervious surface hydrology using bioretention in North Carolina and Maryland. *Journal of Hydrologic Engineering*, *14*, 407–415.

Liu, R., & Fassman-Beck, E. (2017). Hydrologic experiments and modeling of two laboratory bioretention systems under different boundary conditions. Frontiers of environmental science. *Engineering*, *11*, 10.

Liu, W., Chen, W., & Peng, C. (2015). Influences of setting sizes and combination of green infrastructures on community's stormwater runoff reduction. *Ecological Modelling*, *318*, 236–244. https://doi.org/10.1016/j.ecolmodel.2014.11.007

Lucke, T., & Nichols, P. W. B. (2015). The pollution removal and stormwater reduction performance of street-side bioretention basins after ten years in operation. *Science of the Total Environment*, *536*, 784–792. https://doi.org/10.1016/j.scitotenv.2015.07.142

Machusick, M., Welker, A., & Traver, R. (2011). Groundwater mounding at a storm-water infiltration BMP. *Journal of Irrigation and Drainage Engineering*, *137*, 154–160.

Mangangka, I. R., Liu, A., Egodawatta, P., & Goonetilleke, A. (2015). Performance characterisation of a stormwater treatment bioretention basin. *Journal of Environmental Management*, *150*, 173–178.

Meng, Y., Wang, H., Chen, J., & Zhang, S. (2014). Modelling hydrology of a single bioretention system with HYDRUS-1D. *The Scientific World Journal*, *2014*.

Newcomer, M. E., Gurdak, J. J., Sklar, L. S., & Nanus, L. (2014). Urban recharge beneath low impact development and effects of climate variability and change. *Water Resources Research*, *50*, 1716–1734. https://doi.org/10.1002/2013wr014282

Petrides, A., Stewart, R. D., Bower, R., Cuenca, R., & Wolcott, B. (2014). Case study: Scaling recharge rates from pilot projects of managed artificial aquifer recharge in the Walla Walla Basin, Oregon. *Journal of Hydrologic Engineering*, *0*. 05014028. doi:https://doi.org/10.1061/(ASCE)HE.1943-5584.0001102

Raats, P., & Gardner, W. (1971). Comparison of empirical relationships between pressure head and hydraulic conductivity and some observations on radially symmetric flow. *Water Resources Research*, *7*, 921–928.

Romero, C. C., & Dukes, M. D. (2016). Review of turfgrass evapotranspiration and crop coefficients. *Transactions of the ASABE*, *59*, 207–223. https://doi.org/10.13031/trans.59.11180

Schaap, M. (1999). Rosetta Lite Version 1.0. Predicting soil hydraulic parameters from basic data. US Salinity Laboratory, USDA/ARS, Riverside, CA.

Schaap, M. G., Leij, F. J., & van Genuchten, M. T. (1998). Neural network analysis for hierarchical prediction of soil hydraulic properties. *Soil Science Society of America Journal*, *62*, 847–855.

Shuster, W., Gehring, R., & Gerken, J. (2007). Prospects for enhanced groundwater recharge via infltration of urban storm water runoff: A case study. *Journal of Soil and Water Conservation*, *62*, 129–137.

Simunek, J., & Sejna, M. (2011). The HYDRUS software package for simulating the two-and three-dimensional movement of water, heat, and multiple solutes in variably-saturated media. In: Technical manual, PC-Progress, pp: 230.

Stewart, R. D., Moreno, D., & Selker, J. S. (2015). Quantification and scaling of infiltration and percolation from a constructed wetland. *Journal of Hydrologic Engineering*, *20*. 04015007. doi:https://doi.org/10.1061/(ASCE)HE.1943-5584.0001164

Thomas, B. F., & Vogel, R. M. (2011). Impact of storm water recharge practices on Boston groundwater elevations. *Journal of Hydrologic Engineering*, *17*, 923–932.

Toran, L., & Jedrzejczyk, C. (2017). Water level monitoring to assess the effectiveness of stormwater infiltration trenches. Environmental & Engineering. *Geoscience*, *23*, 113–124.

Winston, R. J., Dorsey, J. D., & Hunt, W. F. (2016). Quantifying volume reduction and peak flow mitigation for three bioretention cells in clay soils in northeast Ohio. *Science of the Total Environment*, *553*, 83–95.

Yang, H., Florence, D., McCoy, E., Dick, W., & Grewal, P. (2009). Design and hydraulic characteristics of a field-scale bi-phasic bioretention rain garden system for storm water management. *Water Science and Technology*, *59*, 1863–1872.

Zhang, K., & Chui, T. F. M. (2017). Evaluating hydrologic performance of bioretention cells in shallow groundwater. *Hydrological Processes*. https://doi.org/10.1002/hyp.11308

SUPPORTING INFORMATION

Additional Supporting Information may be found online in the supporting information tab for this article.

How to cite this article: Stewart RD, Lee JG, Shuster WD, Darner RA. Modelling hydrological response to a fully-monitored urban bioretention cell. *Hydrological Processes*. 2017;31:4626–4638. https://doi.org/10.1002/hyp.11386